Int. J. Solids Structures Vol. 20, No. 9/10, pp. 863–880, 1984
Printed in the U.S.A.

0020-7683/84 $3.00 + .00
Pergamon Press Ltd.

BUCKLING, POSTBUCKLING, AND CRIPPLING OF MATERIALLY NONLINEAR LAMINATED COMPOSITE PLATES†

R. R. ARNOLD and J. MAYERS
Stanford University, Stanford, CA 94305, U.S.A.

(*Received* 28 *July* 1983)

Abstract—With advanced composite materials expected to appear to a greater and greater extent in aircraft primary structure, their inherent weight-savings attractiveness is enhanced by permitting relatively lightly loaded plate elements to operate in the postbuckled state. A theoretical development and analysis procedure is presented for prediction of buckling, postbuckling and crippling loads in laminated composite plates. Specific application is made to a number of simply supported, graphite epoxy plates with geometric and material properties corresponding to those included in several experimental programs, the results of which, in the form of load-shortening curves, have been reported in the literature. With the effects of transverse shear and material nonlinearity combined with the maximum-strain failure criterion included in the theoretical analysis, good agreement is obtained with the experimental results for initial buckling, postbuckling stiffness and failure (crippling). The theory and analysis described herein can be used as an aid in the design process, particularly in the isolation of candidate laminates without resorting to extensive and costly test programs.

NOTATION

$A_{ij}(i,j = 1, 2, 6)$	membrane stiffnesses from classical lamination theory
a_1, b_1	arbitrary interlaminar shear coefficients
b	plate width
$B_{ij}(i,j = 1, 2, 6)$	membrane bending stiffnesses from classical lamination theory
$D_{ij}(i,j = 1, 2, 6)$	bending stiffness from classical lamination theory
E_{l_k}, E_{t_k}	longitudinal and transverse Young's moduli of the kth lamina, respectively
E_S	secant modulus of the deformation theory of plasticity
E_{11}, E_{22}	equivalent elastic moduli for a laminated composite in plate axes coordinates
e_i, f_i, g_i	arbitrary displacement coefficients
e	subscript denoting elastic materials
$\bar{e}$	vector of arbitrary x-displacement coefficients
$f_{A_{ijk}}, f_{B_{ijk}}, f_{H_{ijk}}, f_{D_{ijk}}$	compliance ratio factors defined by eqn (50)
F^*	Reissner integrand defined by eqn (1)
F'	stress-energy density
F'_{fm_k}	stress-energy density of the kth lamina as a function of inplane stresses in material coordinates
F'_{m_k}	stress-energy density of kth layer of matrix material
G_{l_k}	inplane shear modulus relative to material axes coordinates
G_m	matrix material shear modulus
G_{12}	equivalent inplane shear modulus for a laminated composite plate relative to material axes coordinates
h	laminate thickness
h_{pij}	arbitrary inplane stress coefficients
$K_{l_k}, K_{t_k}, K_{lt_k}, K_m$	Ramberg–Osgood type parameters for kth lamina inplane and matrix material constitutive relations, respectively
k	kth lamina
L	plate length
m	number of half-buckle wavelengths in x-direction
N	total number of lamina
n	number of half-buckle wavelengths in y-direction
$n_{l_k}, n_{t_k}, n_{lt_k}, n_m$	Ramberg–Osgood type constants for kth lamina inplane and matrix material constitutive relations, respectively
N^{cr}_{cl}, N^{cr}_{wo}	buckling load—classical theory (without transverse shear)
N^{cr}, N^{cr}_w	buckling load—present theory (with transverse shear)
N^{cr}_f	experimental buckling load
N^{cc}_f	experimental crippling load
N^{cc}	crippling load—present theory
N_x, N_y, N_{xy}	inplane stress resultants

†The material contained herein is based in part on a dissertation submitted by the first author to Stanford University in partial fulfillment of the requirements for the Ph.D. degree.

$\bar{P}$ $N \times l$ matrix defined by eqn (46)
p subscript denoting nonlinear elasto–plastic materials
$(\bar{Q}_{ij})_k (i, j = 1, 2, 6)$ transformed reduced stiffnesses of clasical lamination theory
$S_{x_k}^{(0)}, S_{x_k}^{(1)} \ldots$ stiffness ratio factors defined by eqns (41) and (42)
$(\bar{S}_{ij})_k (i, j = 1, 2, 6)$ transformed reduced compliances of classical lamination theory
$t_{f_{mk}}$ lamina thickness
t_{m_k} matrix layer thickness $(z_k - z_{k-1})$
$u^{(0)}, u^{(1)}, u^{(2)}, \ldots$ generalized x-displacements of the polynomic expansion in eqn (43)
u inplane x-direction displacement function
u_k, v_k median surface inplane displacements of kth lamina
v inplane y-direction displacement function
w lateral displacement function
x, y, z plate coordinates
α_{mn} terms of series expansion describing the $x - y$ variations of the u displacement
Δ_x, Δ_y distance between the plate middle surface and the laminate neutral axes in x and y directions, respectively
γ_{xy_k} median surface shearing strains of kth lamina
$\gamma_{yz_k}, \gamma_{zx_k}$ interlaminar shearing strains of kth matrix layer
δ prescribed end-shortening per unit length
δ_{cc} end-shortening per unit length at crippling
δ_{cr} end-shortening per unit length at buckling
ϵ_f fiber strain
ϵ_{max} maximum allowable fiber strain
$\epsilon_{l_k}, \epsilon_{t_k}$ median surface extensional strains of kth lamina relative to material axes coordinates
$\epsilon_{x_k}, \epsilon_{y_k}$ median surface extensional strains of kth lamina relative to plate axes coordinates
ϵ_{eff} strain quantity defined by eqn (20)
$\eta_{l,lt}, \eta_{t,lt}, \eta_{lt,l}, \eta_{lt,t}$ coefficients of mutual influence relative to material axes
ν_{lt}, ν_{tl} major and minor Poisson's ratios relative to material axes
Σ summation sign
σ_{eff} effective stress
$\sigma_{l_k}, \sigma_{t_k}$ median surface extensional stresses of kth lamina in material coordinates
$\sigma_x^{(0)}, \sigma_x^{(1)}, \sigma_x^{(2)}, \ldots$ generalized stresses of the polynomic expansion in eqn (44)
$\sigma_{x_k}, \sigma_{y_k}$ median surface extensional stresses of kth lamina in plate coordinates
τ_{lt_k} median surface shearing stress of the kth lamina in material coordinates
τ_{xy_k} median surface shearing stress of the kth lamina in plate coordinates
τ_{yz_k}, τ_{zx_k} interlaminar shearing stresses of kth matrix layer

INTRODUCTION

The use of advanced composite materials (ACMs) in commercial and military aircraft introduced in the 1970s is, for the most part, based upon predictions of conservative analysis methodologies[1] and/or the results of costly design, test, and redesign procedures. For typical aircraft elements and components such as beam, plate, stiffened panel, and semimonocoque structures, the properties of the fiber-reinforced matrix base material are transformed by the classical lamination theory to equivalent elastic moduli representing the overall laminate. Implicit in this method of design and analysis is the assumption that the new composite part will have the same stiffness and strength characteristics as the metallic part it is to replace. Wherein some weight saving is achieved, an optimized design is not realized because the unique characteristics of the composite material have not been used to full potential. That conservatism in advanced composite design exists is exemplified by the fact that most aircraft applications appear in secondary structures, a direct consequence of cost, confidence, and complexity problems on the one hand and an insufficient research and technology base on the other.

A specific example of the conservative approach is the current standard practice of designing both conventional and composite plate structures under compressive loading by using the buckling load as an indication of structural failure. This practice ignores the significant amount of additional load-carrying capability of postbuckled structural plates. The end result of this practice is an increase in the weight of lightly loaded flight structures above what is needed for safe operation, a design philosophy currently at odds with requirements for significantly improved energy efficiency. For appreciable weight-saving returns, the use of the postbuckling strength of laminated composite plates has direct application to primary structure of helicopters and VSTOL aircraft operating in the low subsonic speed range and to commercial aircraft operating in the high subsonic speed range where loads rarely exceed about 60% of the limit load.

It should also be pointed out that laminated composites possess a number of unique

structural behaviors that are not usually observed in metals. For instance, interlaminar stresses can significantly reduce the buckling and ultimate loads in a laminated composite[2, 3]. Related to this is the effect of fiber orientation and lamination sequence on the composite strength[4]. Material nonlinearities due primarily to the matrix can lead to stress redistribution effects in general. Other stress redistribution effects occur in linear-elastic postbuckled plates; however, they are altered significantly by the material nonlinearities associated with the matrix. The purpose of this paper is to generalize, and both improve qualitatively and extend quantitatively, earlier work by Anderson and Mayers[5] for predicting the postbuckling behavior of composite plates in the elasto-plastic range, including the effects of transverse shear, by removing the restriction to symmetric angle-ply laminates and incorporating a failure criterion for establishing the point of ultimate loading (crippling) on the load-shortening curve of a given composite configuration. The solution procedure of Anderson and Mayers is improved to the point where the equilibrium of resultant forces acting in the plane of the plate, the boundary conditions, and the constitutive relations between average resultant force and average resultant displacement on any section is satisfied in the linear-elastic case; however, the constitutive relation is satisfied only to a good approximation in the elasto-plastic case.

Finally, with regard to failure prediction, the maximum strain criterion is used and shown to be applicable to the prediction of crippling of postbuckled filamentary laminated composite plates. Comparisons with available experimental data show excellent agreement for buckling, postbuckling and crippling.

THEORY

The buckling, postbuckling, and crippling of composite plates requires a theoretical model which is both kinematically and constitutively nonlinear. The complexity of the problem suggests the introduction of the Reissner variational approach[6], one in which both the states of stress and strain (or displacement) can be selected independently. The stress and strain states are each arbitrary, subject to *a priori* satisfaction of prescribed conditions at the plate boundaries. The plate, shown in Fig. 1, consists of N arbitrarily oriented anisotropic laminae of thickness t_{fm_k} with the neutral axes of the laminate located in accordance with classical lamination theory. Unlike classical lamination theory, however, transverse shear effects are included, although no provision is made for the occurrence of discontinuities analogous to either delaminations or debonds. With σ_x, σ_y, τ_{xy}, τ_{yz}, and τ_{zx} representing the components of stress, ϵ_x, ϵ_y, γ_{xy}, γ_{yz}, and γ_{zx} the components of strain, u, v, and w the components of displacement, then a function F'' is defined for the kth layer

$$F'' = \sigma_x\varepsilon_x + \sigma_y\varepsilon_y + \tau_{xy}\gamma_{xy} + \tau_{yz}\gamma_{yz} + \tau_{zx}\gamma_{zx} - F' \tag{1}$$

where, within the framework of large displacement, moderate rotation kinematics, the

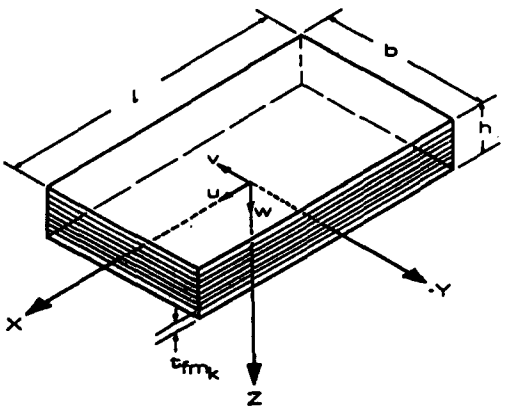

Fig. 1. Laminated composite plate model.

membrane strains are

$$\epsilon_x = \frac{\partial F'}{\partial \sigma_x} = \frac{\partial u}{\partial x} + \frac{1}{2}\left(\frac{\partial w}{\partial x}\right)^2 \tag{2}$$

$$\epsilon_y = \frac{\partial F'}{\partial \sigma_y} = \frac{\partial v}{\partial y} + \frac{1}{2}\left(\frac{\partial w}{\partial y}\right)^2 \tag{3}$$

$$\gamma_{xy} = \frac{\partial F'}{\partial \tau_{xy}} = \frac{\partial u}{\partial y} + \frac{\partial v}{\partial x} + \left(\frac{\partial w}{\partial x}\right)\left(\frac{\partial w}{\partial y}\right) \tag{4}$$

$$\gamma_{yz} = \frac{\partial F'}{\partial \tau_{yz}} = \frac{\partial v}{\partial z} + \frac{\partial w}{\partial y} \simeq \frac{v_k - v_{k-1}}{z_k - z_{k-1}} + \frac{\partial w}{\partial y} \tag{5}$$

$$\gamma_{zx} = \frac{\partial F'}{\partial \tau_{zx}} = \frac{\partial u}{\partial z} + \frac{\partial w}{\partial x} \simeq \frac{u_k - u_{k-1}}{z_k - z_{k-1}} + \frac{\partial w}{\partial x}. \tag{6}$$

It should be noted that these strain-displacement relations apply to each individual lamina and terms which provide for bending in the laminate (for example, $\epsilon_x \sim \partial^2 w/\partial x^2$) are accounted for in the through-thickness processes inherent in basic lamination theory. The Reissner variational principle may be stated as follows: "Among all states of stress and displacement which satisfy the boundary conditions of prescribed surface displacement the actually occurring state of stress and displacement is determined by the variational equation

$$\delta\left\{\int\int\int_V F'' \,\mathrm{d}V - \int\int_S (\bar{p}_x u + \bar{p}_y v + \bar{p}_z w)\,\mathrm{d}S\right\} = 0 \tag{7}$$

where $\bar{p}_x$, $\bar{p}_y$, and $\bar{p}_z$ are prescribed surface tractions on S."

For the present investigation, uniaxially compressed plates under prescribed end-shortening are of interest; hence, the variational equation reduces to the form

$$\delta\left\{\int\int\int_V F'' \,\mathrm{d}V\right\} = 0. \tag{8}$$

Completion of the variational process implied in (8) (see Ref. [7]) shows that the vanishing of the volume integral requires satisfaction of both the lamina equilibrium equations

$$t_{fm_k}\left(\frac{\partial \sigma_{x_k}}{\partial x} + \frac{\partial \tau_{xy_k}}{\partial y}\right) + (\tau_{zx_k} - \tau_{zx_{(k-1)}}) = 0 \tag{9}$$

$$t_{fm_k}\left(\frac{\partial \sigma_{y_k}}{\partial y} + \frac{\partial \tau_{xy_k}}{\partial x}\right) + (\tau_{yz_k} - \tau_{yz_{(k-1)}}) = 0 \tag{10}$$

$$\sum_{k=1}^{N} t_{fm_k}\left\{\frac{\partial}{\partial x}\left[\sigma_{x_k}\left(\frac{\partial w}{\partial x}\right) + \tau_{xy_k}\left(\frac{\partial w}{\partial y}\right)\right] + \frac{\partial}{\partial y}\left[\sigma_{y_k}\left(\frac{\partial w}{\partial y}\right)\tau_{xy_k}\left(\frac{\partial w}{\partial x}\right)\right]\right\} + \sum_{k=1}^{(N-1)} t_{m_k}\left(\frac{\partial \tau_{zx_k}}{\partial x} + \frac{\partial \tau_{yz_k}}{\partial y}\right) = 0 \tag{11}$$

and the lamina stress-displacement relations given by (2)–(6). To account for material nonlinearity in each anisotropic lamina, a modified Ramberg–Osgood[8] constitutive

formulation is introduced. Thus, the biaxial stress–strain relations are

$$\epsilon_{l_k} = \left\{ \frac{\sigma_l}{E_l} - \frac{\nu_{tl}}{E_t}\sigma_t + \frac{\eta_{l,lt}}{G_{lt}}\tau_{lt} + K_l\left(\frac{\sigma_l}{E_l}\right)^{n_l} - \underline{M_{tl}\left(\frac{\sigma_t}{E_t}\right)^{n_t}} \right\}_k \tag{12}$$

$$\epsilon_{t_k} = \left\{ \frac{\sigma_t}{E_t} - \frac{\nu_{lt}}{E_t}\sigma_l + \frac{\eta_{t,lt}}{G_{lt}}\tau_{lt} + K_t\left(\frac{\sigma_t}{E_t}\right)^{n_t} - \underline{M_{lt}\left(\frac{\sigma_l}{E_l}\right)^{n_l}} \right\}_k \tag{13}$$

$$\gamma_{lt_k} = \left\{ \frac{\tau_{lt}}{G_{lt}} + \frac{\eta_{lt,l}}{E_l}\sigma_l + \frac{\eta_{lt,t}}{E_t}\sigma_t + K_{lt}\left(\frac{\tau_{lt}}{G_{lt}}\right)^{n_{lt}} \right\}_k \tag{14}$$

where subscripts l and t represent fiber direction and perpendicular-to-fiber direction, respectively. The underlined terms in (12) and (13) correspond to the induced nonlinear lateral strains. To establish confidence in their elasto-plastic stress-energy density for introduction into the Reissner principle formulation, Anderson and Mayers correlated theoretical prediction of biaxial strain response with test data obtained using off-axis specimens in tension. The high degree of correlation obtained suggests that the strains (12) and (13) can be approximated by setting $M_{tl} = M_{lt} = 0$.

For the matrix material, which is assumed isotropic, the Ramberg–Osgood relations are taken as

$$\gamma_{yz_k} = \left\{ \frac{\tau_{yz}}{G_m} + K_m\left(\frac{\tau_{yz}}{G_m}\right)^{n_m} \right\}_k \tag{15}$$

$$\gamma_{zx_k} = \left\{ \frac{\tau_{zx}}{G_m} + K_m\left(\frac{\tau_{zx}}{G_m}\right)^{n_m} \right\}_k. \tag{16}$$

With the definition of a suitable stress-energy density function F', application of the variational principle will produce both the equilibrium and stress-displacement relations. With some modification to the form presented by Anderson and Mayers, the inplane stress-energy density function (F'_{fm_k}) is written as the sum of a plastic portion

$$\begin{aligned} F'_{fm_{pk}} = \Bigg\{ & \frac{K_l}{(n_l+1)E_l}(\epsilon_{eff})^{(n_l-1)}(\sigma_l^2 - \nu_{tl}\sigma_l\sigma_t + \underline{\underline{\eta_{tl,l}\sigma_l\tau_{lt}}}) \\ & + \frac{K_t}{(n_t+1)E_t}(\epsilon_{eff})^{(n_t-1)}(\sigma_t^2 - \nu_{lt}\sigma_l\sigma_t + \underline{\underline{\eta_{lt,t}\sigma_t\tau_{lt}}} \\ & + \underline{\frac{1}{2}\left(\frac{3}{4}\cdot\frac{1}{(1+\nu_{lt})}\cdot\frac{1}{(1+\nu_{tl})}\right)^{(1-n_{lt})/2}\cdot\frac{K_{lt}}{(N_{lt}+1)G_{lt}}(\epsilon_{eff})^{(n_{lt}-1)}} \\ & \cdot (\tau_{lt}^2 + \underline{\underline{\eta_{t,lt}\sigma_t\tau_{lt} + \eta_{l,lt}\sigma_l\tau_{lt}}}) \Bigg\}_k \end{aligned} \tag{17}$$

and an elastic portion

$$\begin{aligned} F'_{fm_{ek}} = \frac{1}{2}\Bigg\{ & \frac{\sigma_l^2}{E_l} + \frac{\sigma_t^2}{E_t} - \left(\frac{\nu_{lt}}{E_l} + \frac{\nu_{tl}}{E_t}\right)\sigma_l\sigma_t + \frac{\tau_{lt}^2}{G_{lt}} \\ & + \underline{\underline{\left(\frac{\eta_{l,lt}}{G_{lt}} + \frac{\eta_{lt,t}}{E_t}\right)\sigma_l\tau_{lt} + \left(\frac{\eta_{t,lt}}{G_{lt}} + \frac{\eta_{lt,t}}{E_t}\right)\sigma_t\tau_{lt}}}\Bigg\}_k \end{aligned} \tag{18}$$

or

$$F'_{fm_k} = F'_{fm_{ek}} + F'_{fm_{pk}} \tag{19}$$

where the effective strain is defined as

$$\epsilon_{eff_k} = \frac{1}{\sqrt{E_l E_t}}\left\{\frac{E_l}{E_l}\sigma_l^2 + \frac{E_l}{E_t}\sigma_t^2 - (\nu_{lt}+\nu_{lt})\sigma_l\sigma_t + \underline{\left[3\cdot\frac{1}{2(1+\nu_{lt})}\cdot\frac{1}{2(1+\nu_{lt})}\right]\frac{E_l E_t}{G_{lt}}}\right.$$
$$\left.\times\left(\tau_{lt}^2 + \underline{\underline{\frac{\eta_{l,lt}+\eta_{lt,l}}{E_l}\sigma_l\tau_{lt} + \frac{\eta_{t,lt}+\eta_{lt,t}}{E_t}\sigma_t\tau_{lt}}}\right)\right\}_k^{1/2}. \tag{20}$$

The stress-energy density in the earlier work by Anderson and Mayers does not include the term singly underlined in (17). This additional term has been added to insure that the reduction of (17) to an isotropic formulation is consistent with the deformation theory of plasticity for an incompressible isotropic solid. Similarly, the singly underlined constant in (20) must be included in the current approach as well. The doubly underlined terms in (17), (18), and (20), not present in the earlier work of Anderson and Mayers, are required to extend the theory from orthotropic to anisotropic materials.

For the isotropic case where $E_l = E_t = E$, $G_{lt} = G_m = G$, $\nu_{lt} = \nu_{tl} = \nu$, $n_{lt} = n_l = n_t = n$, $K_{lt} = K_l = K_t = K$, then

$$F' = \frac{1}{2}\left(\frac{\sigma_{eff}^2}{E}\right) + EK\left(\frac{1}{n+1}\right)\left(\frac{\sigma_{eff}}{E}\right)^{n+1} \tag{21}$$

where

$$\sigma_{eff} = \{\sigma_x^2 + \sigma_y^2 - \sigma_x\sigma_y + 3\tau_{xy}^2\}^{1/2} = E_S\epsilon_{eff} \tag{22}$$

$$\epsilon_{eff} = \frac{2}{\sqrt{3}}\left\{\epsilon_x^2 + \epsilon_y^2 + \epsilon_x\epsilon_y + \frac{\gamma_{xy}^2}{4}\right\}^{1/2} \tag{23}$$

and σ_{eff} is the effective stress, ϵ_{eff} the effective strain, and E_S the corresponding uniaxial stress–strain curve secant modulus of the J_2 or secant modulus deformation theory of plasticity. For the matrix material,

$$F'_{m_{e_k}} = \frac{1}{2}\left\{\frac{\tau_{zx}^2}{G_m} + \frac{\tau_{yz}^2}{G_m}\right\}_k \tag{24}$$

$$F'_{m_{pk}} = \left\{\frac{K_m}{(n_m+1)G_m}(\tau_{zx}^2 + \tau_{yz}^2)^{(n_m+1)/2}\right\}_k \tag{25}$$

$$F'_{m_k} = F'_{m_{e_k}} + F'_{m_{pk}}. \tag{26}$$

It can be shown that the definitions of F'_{fm_k} and F'_{m_k} reduce identically to the isotropic formulation and satisfy the generalized constitutive relations (2)–(6).

MAXIMUM STRAIN FAILURE CRITERION

To predict the point of ultimate load (crippling) on a load-shortening curve the maximum strain criterion has been introduced into the analysis. To justify the applicability of the maximum strain criterion in the present study, reference is made to the experimental data of Tennyson[9] with tubular composite specimens. Shown in Fig. 3 are the experimental results of Tennyson compared with the analytical work of Craddock and Champagne[10] for various other failure theories. The maximum strain criterion, which was not considered in either of the other works, compares with the test data quite well as can be observed. Shown in Fig. 4 is an enlarged plot of Fig. 3 with just the maximum strain theory compared with test data. It can be seen that for wrap angles between 34° and 52° the mode of failure is shear. For angles less than 34° or greater than 52° the mode of failure is transverse tension.

If, however, the matrix material were to be highly nonlinear (which is often the case) then the "shear" curve would rise and transverse tension would be the principle mode of

failure. For angle-plies greater than $\pm 40°$, it is noted that the data appear shifted by about 2–4°. This is most likely due to manufacturing tolerances in the wrap angle. In tests performed at Ford Aerospace for a similar size tube and graphite epoxy tape it has been found that tubes supposedly belt wrapped at 60° were observed actually to have a wrap angle of 56–58°[11]. When these adjustments are made to the test data, then the correlation with the maximum strain theory is almost exact over the entire range of wrap angles. The test results discussed so far have concentrated on failure associated with the matrix material itself. In the case of the fiber the most commonly observed failure mode is uniaxial tension. Indeed, all the various failure theories produce the same predicted failure load when the load is aligned with the fiber.

The maximum strain failure criterion, like the other failure criteria, is phenomenological in nature. That is to say, the exact mechanism (or physics) of failure is not treated; rather, the observed behavior is modeled with gross macroscopic measureable responses. In this context, the worth of any failure theory must be determined by comparison with actual test data. The maximum strain failure criterion seems to perform very well for laminated composites in which both fiber and matrix are relatively brittle. As pointed out by Grimes and Whitney[12], the maximum strain failure criterion should be accurate as long as the nonlinear shear strain components are small and do not interact with normal strains.

It should also be noted that the maximum strain failure criterion is operationally simple to use, requires the availability of only limited test data, and can be used to predict the actual mode of failure; that is, fiber failure or matrix failure in tension or shear. Other failure theories based upon strengths (for instance, Tsai and Wu[13]) produce a failure surface for which no physically plausible failure mode can be associated. For relatively homogeneous but orthotropic materials such as ATJ-S or pyrolytic graphite, etc. the tensorial theories based on strength are generally more accurate.

APPLICATION TO A SPECIALLY ORTHOTROPIC LAMINATED COMPOSITE PLATE

The analysis undertaken is concentrated on specially orthotropic plates and plates which can be considered as reasonably specially orthotropic (D_{16}/D_{22} and $D_{26}/D_{22} \ll D_{66}/D_{22}$). Reliable experimentally determined load-shortening curves including prebuckling, buckling, postbuckling, and crippling data, exist only for such plates as exemplified by the investigations of Spier *et al.*[14–18].

The use of the Reissner variational theorem provides differential equations of equilibrium and stress-displacement compatibility that must be integrated over the volume of the plate. As a consequence, in effecting an approximate solution, both the equilibrium and stress-displacement equations are satisfied over the volume but not necessarily at a point. If it were possible to construct the exact solution for both stresses and displacements, then equilibrium and stress-displacement equations would also be satisified at every point. In application to a uniformly compressed plate with straight unloaded edges, it is observed that along any $x =$ constant or $y =$ constant line, including the plate edges, the internal resultant forces (N_x, N_y, N_{xy}) are given by

$$N_x = \int_0^b \frac{1}{h} \sum_{k=1}^{N} \sigma_{x_k} t_{fm_k} \, dy = \text{constant} \tag{27}$$

$$N_y = \int_0^L \frac{1}{h} \sum_{k=1}^{N} \sigma_{y_k} t_{fm_k} \, dx = 0 \tag{28}$$

$$N_{xy} = \int_0^b \frac{1}{h} \sum_{k=1}^{N} \tau_{xy_k} t_{fm_k} \, dy = \int_0^L \frac{1}{h} \sum_{k=1}^{N} \tau_{xy_k} t_{fm_k} \, dx = 0. \tag{29}$$

Judicious choice of stress and displacement functions is essential in applying the variational formulation of Reissner; however, a firm judgment as to the accuracy of the solution can

only be made by comparison to other established numerical techniques. For instance, Anderson and Mayers[5] used mathematically rather than physically desirable membrane functions, thereby only approximately satisfying the membrane displacement boundary conditions and the statics conditions (27)–(29). As a result, their solutions fell short of exact static equilibrium satisfaction along all x and y cross sections of the plate, a lack of rigor removed in the present application. Nevertheless, solution acceptability was guided by correlation of results for the predicted ratio of postbuckling stiffness to initial stiffness with established results obtained from load-shortening curves for isotropic and angle-plied ($\pm\theta$) laminated plates.

The kth lamina displacement functions for a simply supported plate with straight unloaded edges free to move in the plane of the plate are

$$u_k = \delta x + e_{11}\sin\frac{2m\pi x}{L}\cos\frac{2n\pi y}{b} + z_k e_{21}\sin\frac{m\pi x}{L}\cos\frac{n\pi y}{b} \tag{30}$$

$$v_k = f_{11}y + f_{12}\sin\frac{2n\pi y}{b}\cos\frac{2m\pi x}{L} + z_k f_{21}\sin\frac{n\pi y}{b}\cos\frac{m\pi x}{L} \tag{31}$$

$$w = g_1\cos\frac{m\pi x}{L}\cos\frac{n\pi y}{b} \tag{32}$$

where e_{11}, f_{11}, f_{12}, etc. are unknown amplitude coefficients to be determined from the variational analysis. These functions are required in order to insure that the desired geometric boundary conditions are satisfied; i.e.

$$u_k = \pm\delta(L/2) \quad \text{at} \quad x = \pm L/2 \tag{33}$$

$$v_k = \pm f_{11}(b/2) \quad \text{at} \quad y = \pm b/2 \tag{34}$$

$$w = 0 \quad \text{at} \quad x = \pm L/2, y = \pm b/2. \tag{35}$$

The kth lamina stress functions are

$$\sigma_{x_k} = S^{(0)}_{x_k}\left(h_{111} + h_{112}\cos\frac{2n\pi y}{b} + h_{113}\cos\frac{m\pi x}{L}\cos\frac{n\pi y}{b}\right) + S^{(1)}_{x_k} z_k h_{121}\cos\frac{m\pi x}{L}\cos\frac{n\pi y}{b} \tag{36}$$

$$\sigma_{y_k} = S^{(0)}_{y_k}\left(h_{211}\cos\frac{2m\pi x}{L} + h_{212}\cos\frac{m\pi x}{L}\cos\frac{n\pi y}{b}\right) + S^{(1)}_{y_k} z_k h_{221}\cos\frac{m\pi x}{L}\cos\frac{n\pi y}{b} \tag{37}$$

$$\tau_{xy_k} = S^{(0)}_{xy_k}\left(h_{311}\sin\frac{2m\pi x}{L}\sin\frac{2n\pi y}{b}\right) + S^{(1)}_{xy_k} z_k h_{321}\sin\frac{m\pi x}{L}\sin\frac{n\pi y}{b} \tag{38}$$

$$\tau_{yz_k} = b_{11} z_k \sin\frac{m\pi x}{L}\cos\frac{n\pi y}{b} \tag{39}$$

$$\tau_{zx_k} = a_{11} z_k \sin\frac{n\pi y}{b}\cos\frac{m\pi x}{L} \tag{40}$$

where the h_{pij}s and a_{11}, b_{11} are determined from the variational procedure and provide for satisfaction of eqns (27)–(29) in the process.

The combination of displacement and stress functions given by eqns (29)–(32) and (36)–(40) represents the most limited set that can be chosen and which still satisfies both geometric boundary conditions and overall membrane equilibrium conditions while providing for the maximum amount of coupling of displacement and stress distributions in the Reissner functional (1).

The quantities $S^{(0)}_{x_k}$, $S^{(0)}_{y_k}$, $S^{(0)}_{xy_k}$, $S^{(1)}_{x_k}$, $S^{(1)}_{y_k}$, $S^{(1)}_{xy_k}$ are stiffness ratio factors introduced to

render the stress distributions applicable to layups other than those reflecting $\pm\theta$-degree fiber orientations. With the stiffness ratio factors each equal to unity, the stress distributions are valid only for isotropic media and $\pm\theta$-degree orthotropic layups, the restriction on the postbuckling analysis conducted by Anderson and Mayers[5]. Thus, the present development represents still another significant improvement of the earlier work to encompass a much wider class of composite laminates.

It should be noticed that when the stiffness ratio factors are unity each layer is assumed to have the same level of membrane stress with the bending contribution being a linear function of z_k. For a general laminated composite this cannot be true. In Fig. 2, a schematic of the strain and stress distributions through the thickness of a typical laminated composite are shown. The strains are assumed to be the sum of a membrane and a linear bending component. However, the stresses are neither linear nor uniform because the stresses are a function of the stiffness of the lamina in that particular direction. Thus, to account for the difference between the actual lamina stress and the assumed laminate average stress,

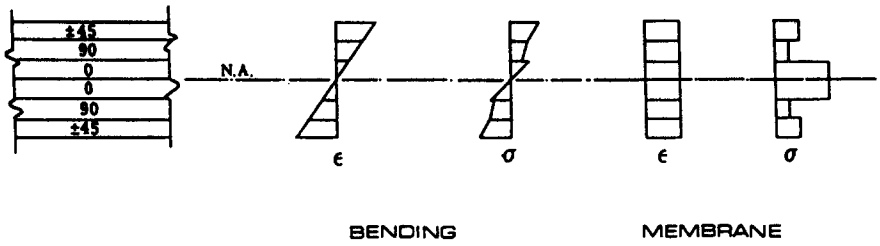

Fig. 2. Typical lamina stress and strain distribution.

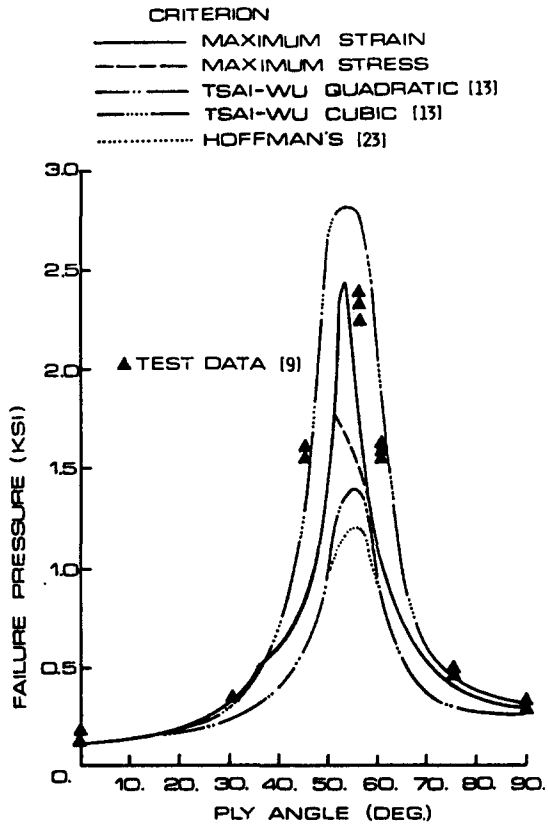

Fig. 3. Comparison of various failure criteria.

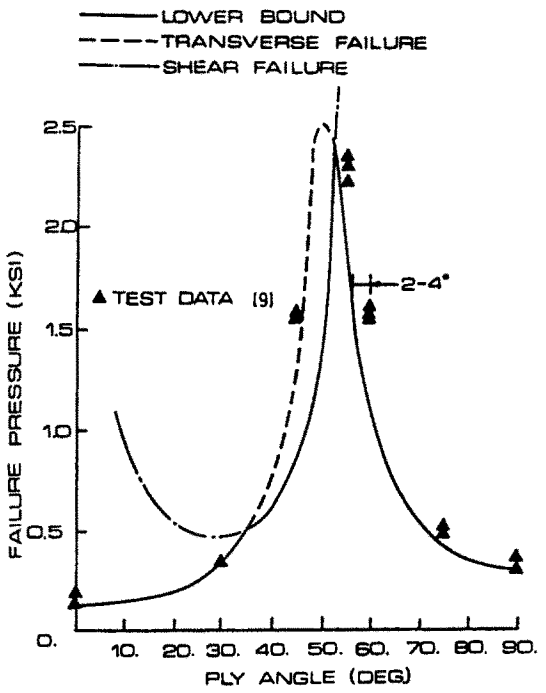

Fig. 4. Comparison of maximum strain criterion with test data from [9].

the stiffness ratio factors

$$S^{(0)}_{x_k} = \frac{(\bar{Q}_{11})_k h}{A_{11}}, \ldots \tag{41}$$

$$S^{(1)}_{x_k} = \frac{(\bar{Q}_{11})_k h^3/12}{D_{11}}, \ldots \tag{42}$$

are introduced as shown in eqns (36)–(40). An alternate procedure would be to take the h_{pij}s and a_{11}, b_{11} different for each lamina, thus increasing significantly the number of variational equations required to effect the solution.

As in Anderson and Mayers[5], following the approach of Durlofsky and Mayers[19] based on their generalization of the sandwich plate model of Hoff[20], the through-thickness variations are taken as polynomic expansions in z

$$u = u^{(0)} + \left(\frac{z}{h}\right)u^{(1)} + \left(\frac{z}{h}\right)^2 u^{(2)} + \ldots \tag{43}$$

$$\sigma_z = \sigma_x^{(0)} + \left(\frac{z}{h}\right)\sigma_x^{(1)} + \left(\frac{z}{h}\right)^2 \sigma_x^{(2)} + \ldots. \tag{44}$$

In vector-matrix notation, the spatial distributions and unknown amplitude coefficients are written, for example, as

$$\hat{u} = \tilde{P}\tilde{\alpha}\vec{e} \tag{45}$$

where

$$\tilde{P} = \begin{bmatrix} 1 & z_1 & z_1^2 & \ldots & z_1^{(l-1)} \\ 1 & z_2 & z_2^2 & \ldots & z_2^{(l-1)} \\ \vdots & \vdots & \vdots & & \vdots \\ 1 & z_N & z_N^2 & \ldots & z_N^{(l-1)} \end{bmatrix} \tag{46}$$

and N = number of lamina. Also

$$\hat{\alpha} = \begin{bmatrix} \alpha_{11}\alpha_{12}\cdots\alpha_{1r_1} & & & \\ & \alpha_{21}\alpha_{22}\cdots\alpha_{2r_2} & & \\ & & \vdots & \\ & & & \alpha_{m1}\alpha_{m2}\cdots\alpha_{mr_m} \end{bmatrix} \tag{47}$$

where α_{mr_m} are the spatial distribution functions in (30)–(32), and

$$\hat{e} = \{e_{11}e_{12}\cdots e_{1r_1}e_{21}e_{22}\cdots e_{2r_2}e_{m1}e_{m2}\cdots e_{mr_m}\}. \tag{48}$$

It is also noted that the application of the Reissner variational theorem leads to the lamina stress–strain relations being established in terms of compliances; that is,

$$\epsilon_{x_k} = (\bar{S}_{11})_k\sigma_{x_k} + (\bar{S}_{12})_k\sigma_{y_k} + (\bar{S}_{13})_k\tau_{xy_k}. \tag{49}$$

The lamina summation process leads to a summation of compliances for each laminate. In general, the summation of lamina compliances cannot yield the correct laminate compliance; thus to account for this possible discrepancy, the energy in each layer must be adjusted by the compliance ratio factors.

$$f_{A_{ij_k}} = \frac{(\bar{A}'_{ij})h}{(\bar{S}'_{ij})_k},\quad f_{B_{ij_k}} = \frac{(\bar{B}'_{ij})\frac{h^2}{4}}{(\bar{S}'_{ij})_k},\quad f_{H_{ij_k}} = \frac{(\bar{H}'_{ij})\frac{h^2}{4}}{(\bar{S}'_{ij})_k},\quad f_{D_{ij_k}} = \frac{(\bar{D}'_{ij})\frac{h^3}{12}}{(\bar{S}'_{ij})_k}. \tag{50}$$

For a nonsymmetric laminate, generalization of the work of Anderson and Mayers requires redefinition of the $\bar{P}$ matrix defined in (46). In Ref. [7], the matrix is developed on the basis of the assumption that the middle surface of the plate is coincident with the neutral axis of the laminate. For isotropic materials, unidirectional and symmetric angle ply ($\pm\theta$) laminates this is indeed true. However, for nonsymmetric laminates, the neutral axis and middle surface are not coincident; thus, a proper accounting of the stress distribution requires that $\tilde{P}$ be defined as

$$\tilde{P} = \begin{bmatrix} 1 & z_1-\Delta & (z_1-\Delta)^2 & \cdots & (z_1-\Delta)^{(l-1)} \\ 1 & z_2-\Delta & (z_2-\Delta)^2 & \cdots & (z_2-\Delta)^{(l-1)} \\ \vdots & \vdots & \vdots & & \vdots \\ 1 & z_N-\Delta & (z_N-\Delta)^2 & \cdots & (z_N-\Delta)^{(l-1)} \end{bmatrix} \tag{51}$$

where Δ is the distance from the middle surface of the plate to the neutral axis of the laminate. Additionally, it is noted that the location of the neutral axis in the x-direction may be quite different than the location of the neutral axis in the y-direction. Thus, it is necessary to define analogous terms $\tilde{P}_x$, $\tilde{P}_y$, Δ_x, Δ_y.

RESULTS AND DISCUSSION

The preceding theoretical developments have been programmed on a CDC 7600 computer in order to perform the calculations. To check the accuracy of the linear-elastic theory many different laminate configurations and rectangular plate sizes (including square) have been analyzed. In all such cases, the transverse shear modulus has been set arbitrarily large (that is $G_{12}/G_m \sim 0$) in order to remove the effects of transverse shear and allow comparison with the classical theory for laminated composites (see, e.g. [21]). The results are summarized in Fig. 5 which shows the quantity (N^{cr}/N^{cr}_{cl}) where N^{cr} is the calculated buckling load of the present theory and N^{cr}_{cl} is the classical buckling load. These results are plotted as a function of the number of inplane integration points used in evaluating the assumed stress and displacement distribution functions. It is noted that the present theory is a least 99.3% accurate for 5 or more integration points per quarter wave of the buckled shape and 12 layers or more. In other words the present theory shows that

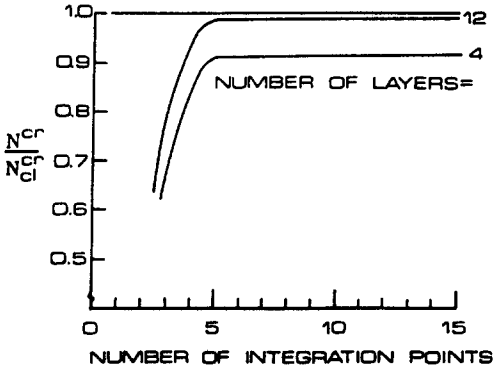

Fig. 5. Convergence of solutions.

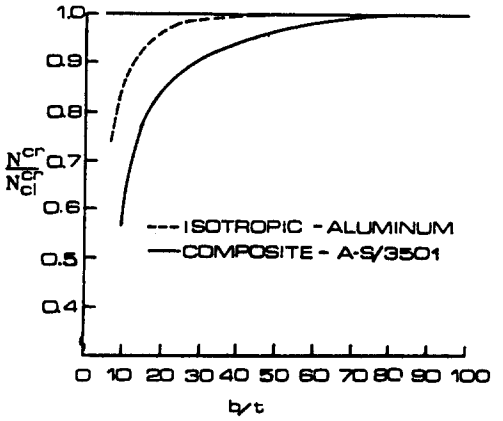

Fig. 6. Effects of transverse shear on initial buckling.

for 5 or more integration points per quarter wave, $N^{cr}/N_{cl}^{cr} \to 1$ as the number of layers approaches infinity.

To establish the effects of transverse shear, a comparison of N_{cl}^{cr}/N_{w}^{cr} for various b/t ratios is shown in Fig. 6. N_{cl}^{cr} refers to the buckling load without the transverse shear effects whereas N_{w}^{cr} refers to the buckling load with transverse shear effects included. A composite layup taken from Spier[14] has been chosen to compare with the results for an isotropic plate. As can be seen in Fig. 6, the effect of transverse shear can be significant for composite plates with b/t ratios as high as even 50. It is also noted that the effect of the transverse shear depends upon both the particular layup and the number of buckle half-wavelengths. The former can be related to the ratios of E_{11}/G_m, E_{22}/G_m, and G_{12}/G_m of the overall laminate; the latter, as in the case of conventional beam and plate structures, depends on the total thickness to wavelength ratios.

It is of extreme interest to note that Spier has stated "... in certain tests, the ultimate loads were less than the corresponding theoretical elastic buckling loads, exposing the futility of using classical buckling theory for laminated plates"[15]. The magnitude of transverse shear effects established through application of the current theoretical analysis justifies Spier's observation. Just how well nonclassical buckling analysis and experiment correlate is demonstrated by the data presented in Tables 1–3. The predictions are those of the present study; the experimental data are those given by Spier in Refs. [14–18]. Whereas the ratio N_f^{cr}/N_{cl}^{cr} ranges from 0.50 to 0.93, the ratio N_f^{cr}/N_w^{cr} ranges from 0.76 to 1.12. Furthermore, if the test corresponding to $N_f^{cr}/N^{cr} = 0.76$ were to be eliminated on the basis of being a questionable point, the range for N_f^{cr}/N_w^{cr} would be 0.89–1.12. Thus, it seems reasonable to conclude that, within the range of scatter to be expected in conducting laminated composite plate testing, the present theory and analysis procedure adequately predict buckling loads for composite plates in the linear elastic range.

Table 1. Predicted buckling loads compared with test data from Ref. [14]

SPECIMEN ID	b/t	Test	Buckling Load (KIPS) Theory (Classical)	Theory (With Shear)	N_t^{cr}/N_{cl}^{cr} Theory (Classical)	N_t^{cr}/N_w^{cr} Theory (With Shear)
3-S1	33.9	2.95	3.12	2.84	.94	1.04
3-S2	33.7	2.95	3.20	2.91	.92	1.01
4-S1	41.5	2.45	2.57	2.38	.95	1.03
4-S2	40.7	2.55	2.74	2.52	.93	1.01
7-S1	32.9	2.82	3.30	2.90	.85	.97
7-S2	32.0	3.00	3.68	3.21	.82	.94

Table 2. Predicted bukling loads compared with test data from Ref. [15]

SPECIMEN NUMBER	B	L (in.)	b (in.)	t (in.)	b/t	Test (lb) [18]	Buckling Load (lb) Theory (Classical)	Theory (With Shear)	N_t^{cr}/N_{cl}^{cr} Theory (Classical)	N_t^{cr}/N_w^{cr} Theory (With Shear)
2A	4	8.0	2.002	.0630	31.8	3,000	3,786	3,252	.79	.92
2B	4	8.0	2.001	.0642	31.2	3,250	4,009	3,424	.81	.95
2C	4	8.0	2.002	.0617	32.5	3,250	3,556	3,072	.91	1.06
4A	8	8.0	2.001	.0838	23.9	6,300	8,015	6,757	.73	.93
4B	8	8.0	2.001	.0821	24.4	6,400	8,101	6,409	.79	1.00
4C	8	8.0	2.007	.0849	23.6	6,350	8,935	6,972	.71	.91
6A	12	8.0	2.001	.1 30	19.4	10,200	15,307	11,020	.66	.93
6B	12	8.0	2.001	.1052	19.0	10,300	16,405	11,590	.63	.89
6C	12	8.0	2.004	.1 31	19.4	12,400	15,423	11,037	.80	1.12
1A	4	12.0	3.000	.0644	46.6	2,300	2,697	2,506	.85	.92
1B	4	12.0	3.000	.0644	46.6	1,900	2,689	2,499	.71	.76
1C	4	12.0	3.000	.0642	46.7	2,250	2,672	2,484	.84	.91
3A	8	12.0	3.000	.0836	35.9	5,100	5,682	5,086	.90	1.00
3B	8	12.0	3.000	.0867	34.6	5,200	6,363	5,627	.82	.92
3C	8	12.0	3.000	.0860	34.9	5,700	6,210	5,502	.92	1.04
5A	12	12.0	3.000	.1057	28.4	9,250	11,098	9,356	.83	.99
5B	12	12.0	3.000	.1066	28.1	10,400	11,383	9,572	.91	1.09
5C	12	12.0	3.000	.0980	30.6	8,000	8,845	7,625	.90	1.05

Table 3. Predicted buckling loads compared with test data from Refs. [17, 18]

SPECIMEN NUMBER	b/t	Test (lb)	Buckling Load (lb) Theory (Classical)	Theory (With Shear)	N_t^{cr}/N_{cl}^{cr} Theory (Classical)	N_t^{cr}/N_w^{cr} Theory (With Shear)	Layup
6B-N[18]	23.9	7,710	9,500	7,454	.81	1.03	$[45/0/-45/90]_{2s}$
5A-N[18]	37.0	5,600	6,000	5,381	.93	1.04	$[45/0/-45/90]_{2s}$
Fig. 6 of [17]	12.4	10,600	21,400	10,176	.50	1.04	$[\pm 45_2/0_{12}/\pm 45]_T$
Fig. 7 of [17]	38.2	4,300	5,000	4,480	.86	.96	$[45/0_2/-45/0_4]_s$
Fig. 10 of [17]	18	8,300	13,300	8,675	.62	.96	$[0_6/\pm 45_2]_s$
Fig. 10 of [17]	28	7,080	8,549	6,987	.83	1.01	$[0_6/\pm 45_2]_s$

Table 4. Predicted fiber strains at experimental value of crippling load

b/t	Layup	$(\delta/\delta_{cr})_e$	N_1^{cr}/N^{cr}	N_1^{cc}/N^{cc}	ϵ_f (%)
32	$[\pm 45/90/0_3]_s$	2.8	.97	1.06	−1.2
41	$[\pm 45/0_3/90]_s$	3.4	1.01	.95	−1.4
34	$[\pm 45/0_3/90]_s$	2.6	1.01	.95	−1.1
37	$[45/0/-45/90]_{2s}$	2.1	1.04	1.07	−0.8
38	$[45/0_2/-45/0_4]_{2s}$	3.0	.96	.98	−0.8
28	$[\pm 45/0_6]_s$	1.8	1.09	1.03	−1.0
36	$[\pm 45/0_4]_s$	2.4	1.00	1.02	−1.1

To the extent that classical theories can account only for linear material behavior, the validity of the present theory, specialized to linear elastic considerations, is established. However, verification of the theory for nonlinear material effects is required. In this regard, the earlier work of Anderson and Mayers[5], in which both isotropic and symmetric angle-plied composites are examined, has confirmed the validity of the current nonlinear material model for at least these cases. Indeed, the present theory reduces to that of Anderson and Mayers for the special cases cited above. For more complex laminated constructions, that is, nonsymmetric and arbitrarily angle-plied laminates, the present theory in its full extent is required. Fortunately, the recent work by Spier *et al.*[14–18] provides the necessary experimental data to verify both the general applicability of the present buckling and postbuckling theory and establish a criterion for the prediction of ultimate (crippling) load.

Given in Table 4 are comparisons of theory and experiment for 7 of the 13 experimental load-shortening curves presented by Spier *et al.*: six of the load-shortening curves are not considered as the respective test specimens reflect plates which either are too thick ($b/t < 18$) or duplicate closely one or more of the seven selected. As can be seen, the ratio of experimental and theoretical results for initial buckling and crippling, respectively, are in excellent agreement in consideration of the scatter to be expected in the testing of laminated composites. The theoretical crippling load has been determined as the load corresponding to the $(\delta/\delta_{cr})_e$ of the experiment and for which the fiber strain shown in the last column of Table 4 satisfies the criterion $0.8\% < \epsilon_{max} < 1.2\%$, the range in which all seven of the test plates fail. Conversely, in the absence of an experimental curve, the prediction procedure would be to construct the theoretical load-shortening curve N/N^{cr} versus δ/δ_{cr} to the point where the calculated maximum fiber strain exceeds 1.0% in compression. It is important to note that the typical B-basis allowable strain (95% confidence, 90% probability) presented in Ref. [1] is 0.83% in compression and 1.15% in tension. Thus, for design purposes, it is recommended that a maximum compressive fiber strain of 0.83% be used in place of the 1.0%.

Comparison of theory with experiment for actual load-shortening curves taken from Spier[14] are shown in Figs. 7–13. The analytical results for the actual nonlinear material behavior are shown with the symbol (×). Only three calculated points in addition to the initial buckling point are determined in view of the relative smoothness of the experimental curve and in the interest of minimizing computational cost. Roughly speaking, the difference in costs between producing a linear-elastic point and an elasto-plastic point is two orders of magnitude.

The final calculated point possesses the same δ/δ_{cr} value as the experiment using, as shown, e.g., in Fig. 7, the abscissa intercept corresponding to an initial prebuckling slope of $E_{11} = 11.1 \times 10^6$ psi, the laminate modulus obtained by Spier through the material testing phase of the experimental program. In view of the data compiled in Table 4 and the typical load-shortening curve correlations obtained in Figs. 7–13, the agreement with Spier's test results can be considered exceptionally good. Nevertheless, it should be pointed out that the plates treated analytically possess straight unloaded edges whereas the experimental plates reflect stress-free unloaded edges. However, the linear-elastic analyses of Banks *et al.*[22] for cross-plied reinforced plastic plates having both types of boundary

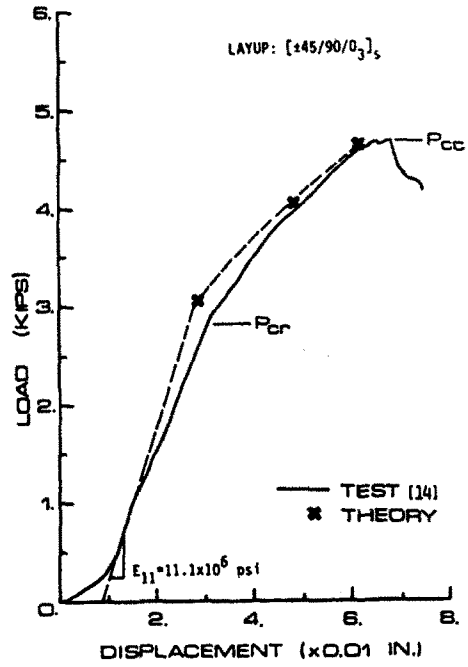

Fig. 7. Predicted load-shortening curve compared with test (specimen 3-S2).

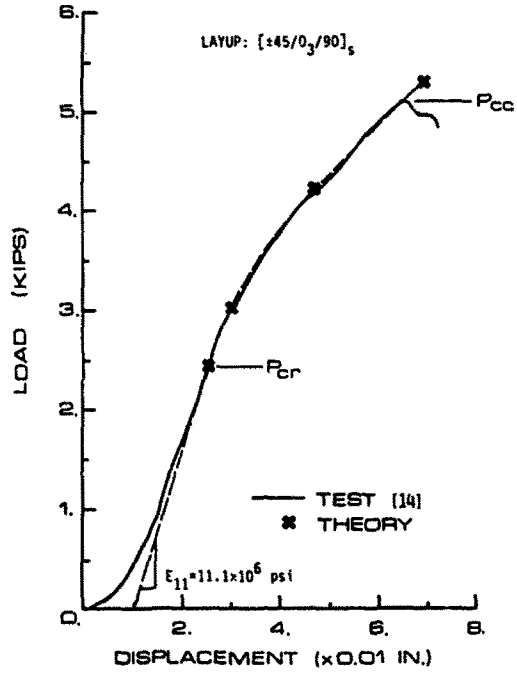

Fig. 8. Predicted load-shortening curve compared with test (specimen 4-S2).

conditions along the unloaded edges show that load-shortening curves are essentially the same in the early postbuckling range ($1 < \delta/\delta_{cr} < 3$). The load-shortening curve in Figs. 7–13 and the data of Table 4 are all in the range $1 < \delta/\delta_{cr} < 3.4$. Thus, it would appear that it is consistent to compare results of the present theoretical analysis with the experimental work of Spier.

In retrospect, both the qualitative and quantitative nature of the correlation of experimental and theoretical results appear to be quite satisfactory. Obviously, some scatter in the test data is to be expected when dealing with composites. As to the theoretical

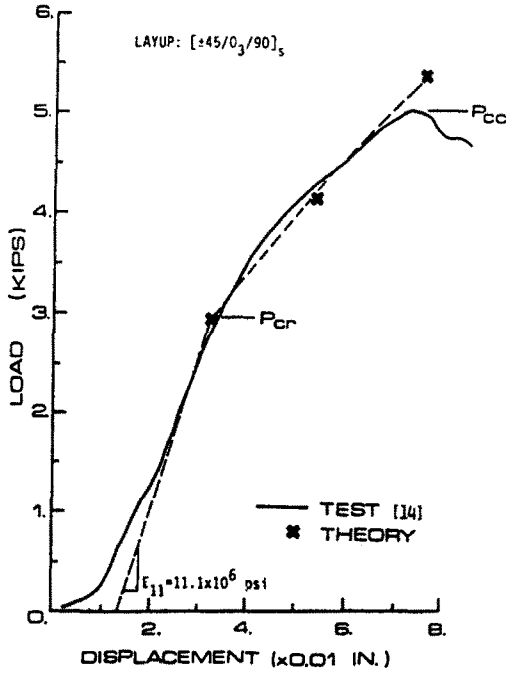

Fig. 9. Predicted load-shortening curve compared with test (specimen 7-S1).

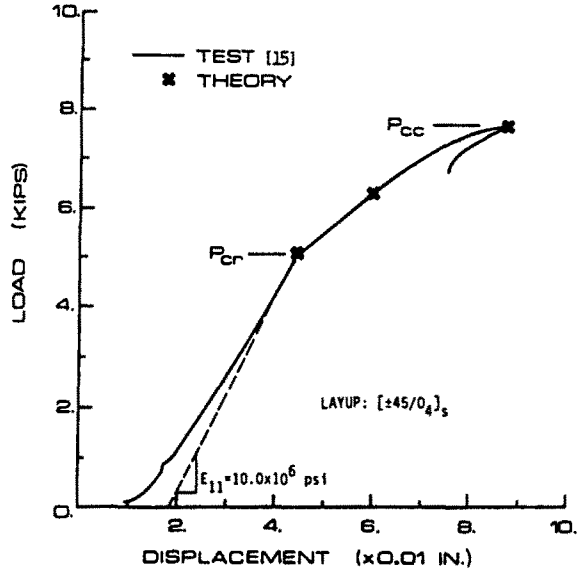

Fig. 10. Predicted load-shortening curve compared with test (specimen 3A).

model itself, the results demonstrate that it is quite capable of recognizing and dealing with all macroscopic kinematical and constitutive effects on plate buckling, postbuckling, and crippling. Certainly, it can be used to identify for the designer those configurations which maximize both initial buckling and crippling loads. Although the particular analyses carried out apply to laminates made of one fiber/matrix system, the theoretical model is capable of treating hybrids (e.g. a combination of graphite and Kevlar epoxy laminae). Finally, it is observed that the mixed variational principle of Reissner, as modified herein to account for elasto-plastic behavior of composites, demonstrates excellent convergence with a near minimum of free variables in the displacement and stress distributions. Specifically, it is noted that all solutions have been effected with only one term in the out-of-plane deflection function.

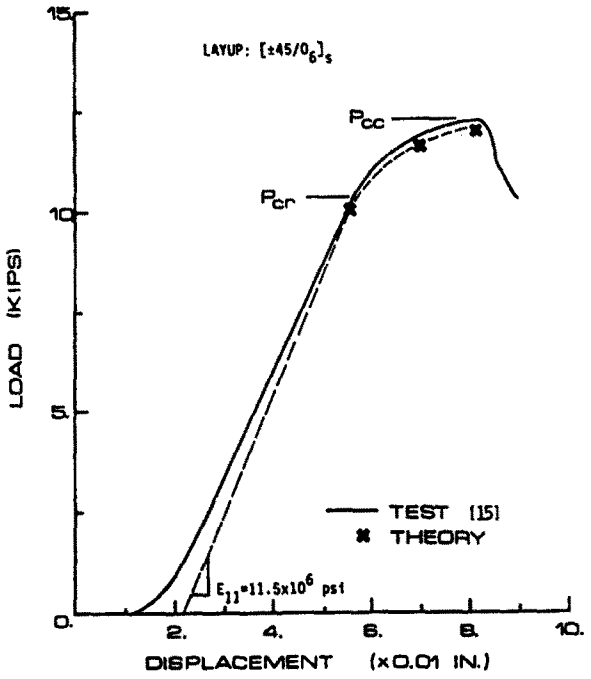

Fig. 11. Predicted load-shortening curve compared with test (specimen 5B).

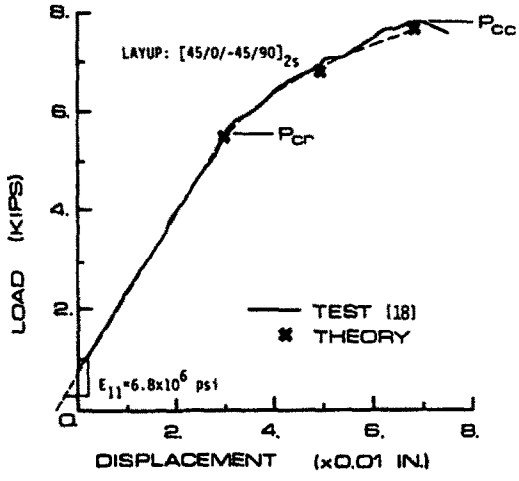

Fig. 12. Predicted load-shortening curve compared with test (specimen 5A-N).

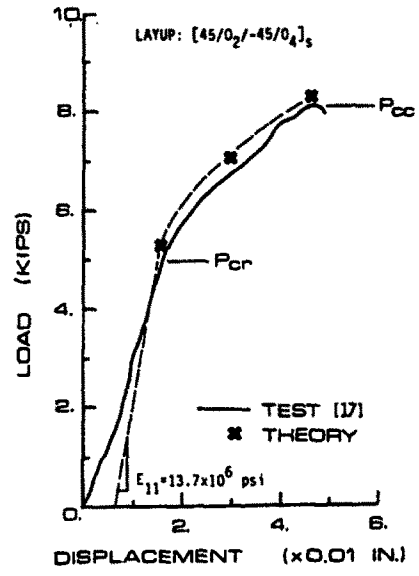

Fig. 13. Predicted load-shortening curve compared with test (specimen F7).

CONCLUDING REMARKS

The theory and available experimental data presented herein show that composite plates have significant postbuckling strength which can and should be utilized in the design process for achieving improved structural efficiency in primary structure. For example, aircraft panels which have compressive loads applied could be designed on the basis of using the ultimate rather than the buckling strength of the panel as the allowable in order to achieve appreciable weight savings. For helicopter fuselage structure and commercial airplane fuselage and empennage structure, load intensities are relatively light; thus, the concept of permitting some buckling and postbuckling at and beyond limit load is not without some justification. Since the material behavior of fiber-reinforced laminated

composites is fundamentally nonlinear, theory and analysis capability has been made available to accurately predict buckling, postbuckling and crippling of composites plates. The theory and analysis developed herein, which both improves and extends earlier work of Anderson and Mayers[5], when combined with the maximum strain failure criterion provide the capability as demonstrated by close prediction of available experimental results providing load-shortening curves to failure. In addition, the transverse shear effects included in the current theory and analysis have resolved to within $\pm 10\%$ the large discrepancy between the classical buckling criterion and experimental results for initial buckling on thirty composite plates.

Acknowledgement—The authors acknowledge with deep appreciation the key contribution of Edward E. Spier, General Dynamics/Convair Division, in establishing experimental buckling, postbuckling, and crippling data for a wide range of graphite/epoxy composite plate structures, the absence of which would have rendered the theoretical analysis results presented herein only speculatively accurate.

REFERENCES

1. Advanced Composites Design Guide, 3rd Edn, 2nd rev. Structures Division, Air Force Flight Dynamics Laboratory, Air Force Systems Command, Wright-Patterson Air Force Base (1976).
2. J. R. Vinson and T. W. Chou, *Composite Materials and Their Use in Structures*, pp. 281–309. Wiley, New York (1975).
3. S. Tang, Interlaminar stresses of uniformly loaded rectangular composite plates. *J. Composite Materials* **10**, 69 (1976).
4. J. M. Whitney and C. E. Browning, Free edge delamination of tensile coupons. *J. Composite Materials* **6**, 300 (1972).
5. R. E. Anderson and J. Mayers, Effects of nonlinear material behavior on postbuckling stiffness of laminated composite plates. *Proc. AIAA Aircraft Systems and Technology Meeting*, New York (1979).
6. E. Reissner, On a variational theorem in elasticity. *J. Math. Phys.* XXIV 90–95 (1950).
7. R. E. Anderson, A variational theorem for laminated composite plates of nonlinear materials and application to postbuckling. Ph.D. Thesis, Stanford University (1978).
8. W. Ramberg and W. R. Osgood, Description of stress strain curves by three paramters. NACA Tech. Note 902 (1934).
9. R. C. Tennyson, D. MacDonald and A. P. Nanyara, Evaluation of the tensor polynomial failure criterion for composite materials. *J. Composite Materials* **12**, 63 (1978).
10. J. N. Craddock and D. J. Champagne, A comparison of failure criteria for laminated composite materials. *Proc. AIAA 23rd Struct. Conf.* (1982).
11. B. Mellberg, Private communication. Ford Aerospace, Palo Alto, California (1982).
12. G. C. Grimes and J. M. Whitney, Degradation of graphite/epoxy composite material because of load induced micromechanical damage. *SAMPE Quart.* (1974).
13. S. Tsai and E. Wu, A general theory of strength for anisotropic materials. *J. Composite Materials* **5**, 58 (1971).
14. E. E. Spier, Local buckling, postbuckling, and crippling behavior of graphite/epoxy short thin walled compression members. Dept. of Navy, Naval Air Systems Command, *Rep. NASC-N*00019-80-*C*00174 (1981).
15. E. E. Spier and F. L. Klouman, Postbuckling behavior of graphite/epoxy laminated plates and channels. *Proc. Army Symp. on Solid Mech.*, Cape Cod (1976).
16. E. E. Speir and F. L. Klouman, Empirical crippling analysis of graphite/epoxy laminated plates. *Composite Materials: Testing and Design, 4th Conf.* ASTM STP-617 (1977).
17. E. E. Spier, On experimental versus theoretical incipient buckling of narrow graphite/epoxy laminated plates. *Proc. Army Symp. on Solid Mech.*, Cape Cod (1976).
18. E. E. Spier, Stability of graphite/epoxy structures with arbitrary symmetrical laminates. *Experimental Mech.* **18**, (1978).
19. H. Durlofsky and J. Mayers, The effects of interlaminar shear on the bending and buckling of fiber-reinforced composite, flat and curved plates. USAAVLABS TR 71-20, AD 728 834 (1971).
20. N. J. Hoff, Bending and buckling of rectangular sandwich plates. NACA Tech. Notes 225 (1950).
21. R. M. Jones, *Mechanics of Composite Materials*. Scripta, Washington, DC (1975).
22. W. M. Banks, J. M. Harvey and J. Rhodes, The nonlinear behavior of composite panels with alternative membrane boundary conditions on the unloaded edges. *Proc. 2nd. Int. Conf. on Composite Materials*, Toronto, Canada (1978).
23. O. Hoffman, The brittle strength of orthotropic materials. *J. Composite Materials* **1** (1967).